International Journal of Minerals, Metallurgy and Materials
Volume 26, Number 2, February 2019, Page 222
https://doi.org/10.1007/s12613-019-1727-7

Investigation on the homogenization treatment and element segregation on the microstructure of a γ/γ′-cobalt-based superalloy

Saeed Aliakbari Sani[1)], *Hossein Arabi*[1)], *Shahram Kheirandish*[1)], *and Golamreza Ebrahimi*[2)]

1) School of Materials and Metallurgical Engineering, Iran University of Science and Technology (IUST), Narmak, Tehran 16846-13114, Iran
2) Materials and Polymers Engineering Department, Faculty of Engineering, Hakim Sabzevari University, Sabzevar 96179-75487, Iran
(Received: 24 April 2018; revised: 5 July 2018; accepted: 13 July 2018)

Abstract: The aim of the present study was to investigate the effect of element segregation on the microstructure and γ′ phase in a γ/γ′ cobalt-based superalloy. Several samples were prepared from a cast alloy and homogenized at 1300°C for different times, with a maximum of 24 h. A microstructural study of the cast alloy using wavelength-dispersive spectroscopic analysis revealed that elements such as Al, Ti, and Ni segregated mostly within interdendritic regions, whereas W atoms were segregated within dendrite cores. With an increase in homogenization time, segregation decreased and the initial dendritic structure was eliminated. Field-emission scanning electron microscopy micrographs showed that the γ′ phases in the cores and interdendritic regions of the as-cast alloy were 392 and 124 nm, respectively. The size difference of γ′ was found to be due to the different segregation behaviors of constituent elements during solidification. After homogenization, particularly after 16 h, segregation decreased; thus, the size, chemical composition, and hardness of the precipitated γ′ phase was mostly uniform throughout the samples.

Keywords: superalloy; segregation; homogenization; microstructure; γ′ phase

1. Introduction

The phenomenon of segregation in superalloys has been frequently reported because of the alloys' multicomponent and nonequilibrium production techniques. In nickel (Ni)-based superalloys, heavy elements such as tungsten (W) and rhenium (Re) tend to accumulate in the dendrite core, whereas aluminum (Al), titanium (Ti), and molybdenum (Mo) preferentially accumulate in interdendritic regions [1–6]. The accumulation of alloying elements can cause the formation of topologically close-packed (TCP) [7–8], η, and Laves phases [9–10] or detrimental γ–γ′ eutectic phases [11–12] during solidification, heat treatment, or service. The formation of undesirable phases results in other defects during thermomechanical treatments [9], and these effects adversely influence the final mechanical properties [8,13–14]. In addition, the proper dispersion of elements and favorable phases—especially γ′ phase—have been reported to be the major parameters affecting the elimination of segregation [15–17].

Segregation can be alleviated in wrought superalloys by application of various controlled thermomechanical treatments. In cast alloys, however, the elimination of segregation is only possible via a homogenization heat treatment. In Ni-based superalloys, heat treatments are usually conducted at temperatures above the γ′-phase solution temperature but lower than the melting point of the alloy (or incipient melting point); this temperature range is called the "homogenization window" [18]. Homogenization is a controlled phenomenon with long-range diffusion. Hence, a proper understanding of the diffusion mechanism of the elements can be important when dealing with segregation phenomena. Many phenomena that occur in metals and alloys, including solidification, precipitation, dissolution, phase transformation, and recrystallization, are strongly related to the phenomenon of element diffusion [19–20].

Recently, a novel group of Co-containing superalloys based on the Co–Al–W system have been introduced; these superalloys are strengthened by an ordered γ′ phase, exhibit

Corresponding author: Hossein Arabi E-mail: arabi@iust.ac.ir

the $L1_2$ structure, and have a stoichiometric composition of $Co_3(Al,W)$ [21]. The morphology and size of the γ′-phase particles and their interface with the γ matrix result in properties similar to those of advanced Ni-based superalloys [22]. The addition of tantalum (Ta), titanium (Ti), and nickel (Ni) to Co–Al–W alloys has been reported to improve the final properties of the resultant alloys [22–25]. Some superalloys of this type have been reported [24–27] to exhibit mechanical properties similar to those of well-known Ni-based superalloys such as Waspaloy, In713, MarM247, and CMSX-2.

Tsunekane *et al*. [28] reported that, during solidification of single-crystalline and polycrystalline cast Co–Al–W alloys, W, Al, and Co were equally distributed within the matrix, although Ta atoms tended to accumulate in the interdendritic region. That is, some Ta atoms remained in the liquid, solidifying during the last stages of solidification. These researchers claimed that casting large, defect-free components with these alloys is possible because of their low degree of elemental segregation. Ding *et al*. [29] and McDevitt [30] reported that, although some Al and Ti atoms segregate in the interdendritic regions of Co–Al–W–Ti alloys, W strongly accumulates inside the dendrite cores. Similarly, a high degree of elemental segregation has been reported in developed multicomponent alloys of Co–Al–W type [31–32]; this segregation can lead to the formation of detrimental phases during heat treatment [32].

Therefore, a homogenization treatment is considered critical for removing the elemental segregation and thereby reducing the amount of undesirable precipitates formed in these alloys, especially on grain boundaries. Although homogenization treatments of such superalloys in the temperature range of 1200–1350°C have been performed by several researchers [25,27,30,33], a precise and systematic investigation of homogenization and its effects on the segregation and microstructure of new Co–Al–W superalloys has yet to be reported. Keeping this in mind, the study of these uncertainties in a multicomponent (Co–Al–W–Ni–Ti–C–B) Co-based superalloy was the prime goal of the present research. For this purpose, a new Co-based alloy was designed and developed and its cast and homogenized microstructures were investigated, mainly to study the possible effects of homogenization treatment on the element segregation, microstructure, and formation of gamma phases in the new γ/γ′-Co-based alloy.

2. Experimental

Raw materials for casting of a Co-based alloy were charged into an alumina crucible, which was subsequently placed in a vacuum induction melting furnace. The furnace was switched on, and a vacuum of 1 Pa was reached; the furnace was then purged with pure argon gas to cast the alloy under a positive pressure. Notably, the choice of elements was based on the following rationale: Al and W elements are required to form γ′ precipitates, whereas the addition of Ti and Ni can enhance the volume fraction of the γ′ phase and improve the mechanical properties of the alloy; carbon (C) and born (B) were added to improve the grain-boundary strength. Investment casting was performed in an alumina mold. The chemical composition of the cast alloy was analyzed by the inductively coupled plasma atomic emission spectroscopy (ICP–OES) method. The carbon content of the cast alloy was measured with a LECO carbon analyzer. The chemical composition of the cast alloy is presented in Table 1. Several samples with dimensions of 1 cm × 1 cm × 1 cm were cut from the cast bar and encapsulated in a quartz tube for the homogenizing treatment. The encapsulated samples were homogenized at 1300°C for 2, 4, 8, 16, or 24 h and then cooled inside the electrical furnace. The aforementioned temperature was selected on the basis of the thermal analysis results of the alloy. The homogenization temperature in this investigation was equal to 0.9 of the alloy's homologous temperature.

Table 1. Chemical composition of the cast Co–Al–W superalloy used in this study

Composition	Content / at%	Content / wt%
Al	9.8	4.11
W	7.4	21.1
Ti	2.7	2.01
Ni	20.4	18.58
C	0.4	0.07
B	0.1	0.01
Co	Bal.	Bal.

Specimens were etched in a solution of 50 mL HCl + 50 mL HNO_3 after being ground and polished. Optical microscopy, scanning electron microscopy (SEM), and field-emission scanning electron microscopy (FE–SEM) were used to characterize the microstructure of the specimens. Also, wavelength-dispersive X-ray spectroscopy (WDS) analysis was performed by electron-probe microanalysis (EPMA; model CAMECA SX-100) to precisely determine the concentration of primary alloying elements (W, Ni, Ti, and Al). WDS analysis of the specimens was performed both at certain points inside the dendrite core and at points in the interdendrite region. Differential scanning calorimetry (DSC) was carried out at a heating/cooling rate of

$10°C \cdot min^{-1}$ under nitrogen protective gas for selected samples. All of the quantitative examinations were accomplished with the Image J software. Vickers microhardness measurements were performed in both regions (core and interdendrite) in all of the samples, along with a compression mechanical test at high temperature (850°C).

3. Results and discussion

3.1. As-cast alloy

The dendritic microstructure generated by the primary dendrites and the secondary dendrites through nonequilibrium solidification of the alloy is presented in Fig. 1(a). The secondary dendrite arm spacing was (39 ± 5) μm. A high-magnification SEM micrograph of the dendritic microstructure (Fig. 1(b)) shows the existence of several whitish precipitates inside the interdendritic regions. Typical energy-dispersive X-ray spectroscopy (EDS) analysis of these precipitates (point A) reveals that the C, W, and Ti contents were high in these areas (Fig. 1(c)). This result might indicate that these regions are MC-type carbides because they are rich in W and Ti. These carbides were relatively coarse, with a Chinese script morphology, and occupied approximately 6% of the volume of the microstructure.

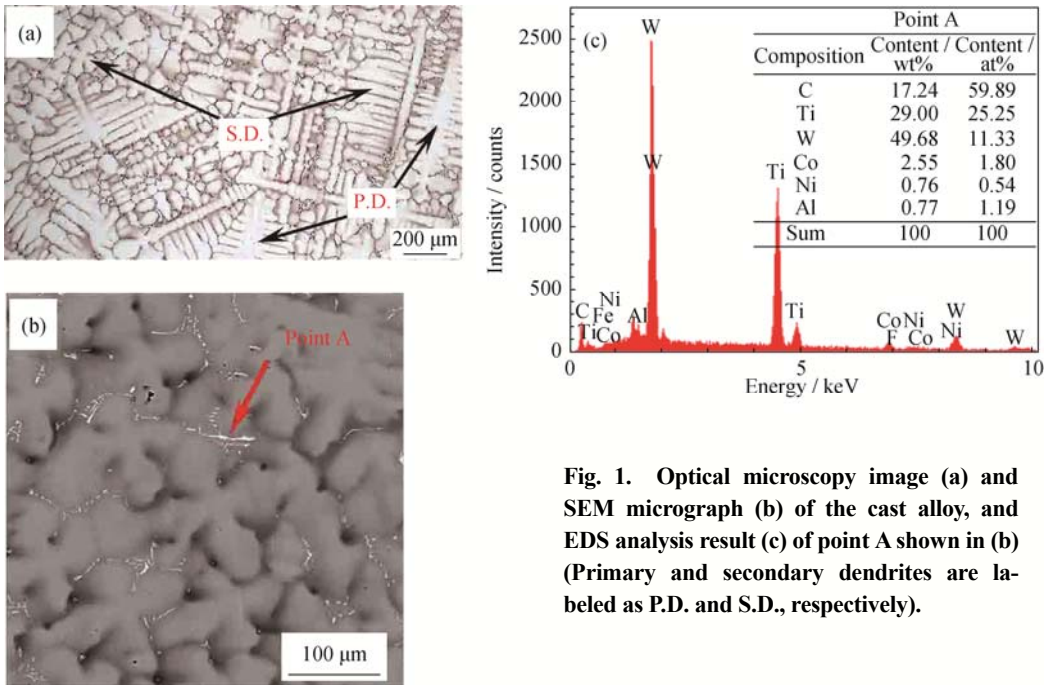

Fig. 1. Optical microscopy image (a) and SEM micrograph (b) of the cast alloy, and EDS analysis result (c) of point A shown in (b) (Primary and secondary dendrites are labeled as P.D. and S.D., respectively).

Fig. 2 shows the X-ray mapping images of the elements in the cast sample. The carbide phases are clearly rich in Ti and W. Closer examination of the carbide-free zones reveals that Ti was highly segregated into interdendritic regions, whereas the content of W in the interdendritic regions was substantially lower. Fig. 2 shows no sign of Al and Ni segregation. A typical microstructure of the cast alloy is shown in Fig. 3(a).

Fig. 3(b) shows a magnified section of the as-cast microstructure. The γ′ phase shown in Fig. 3(b) has a high volume fraction (~75%), and its size varies throughout various regions of the microstructure. The γ′ particles in dendrite cores are smaller than those in the areas adjacent to carbides in the interdendritic region. The reasons behind this difference are discussed in section 3.4.

Thermal analysis revealed that the melting temperature, solidus temperature, and γ′ dissolution temperature of the alloy were 1465, 1366, and 1084°C, respectively. According to the DSC results, the solidification range of this alloy is approximately 100°C. Although the solidification range for ternary Co–Al–W superalloy systems has been reported [25,27–28,34] as being less than 30°C, for quaternary systems, it scarcely exceeds 50°C. Thus, the large solidification range of the alloy is due to either the presence of several elements in the alloy composition (six elements) or a high content of the alloy elements (approximately 41at% or 46wt%), which can enlarge the solidification range [31]. In ternary Co–Al–W superalloys, the γ′ dissolution temperature is less than 1000°C [21,25,35]; however, it can be increased by the addition of alloying elements such as Ni and Ti [34–36]. The γ′ phase is likely formed from the supersaturated matrix during the final stage of solidification at temperatures lower than the precipitation temperature.

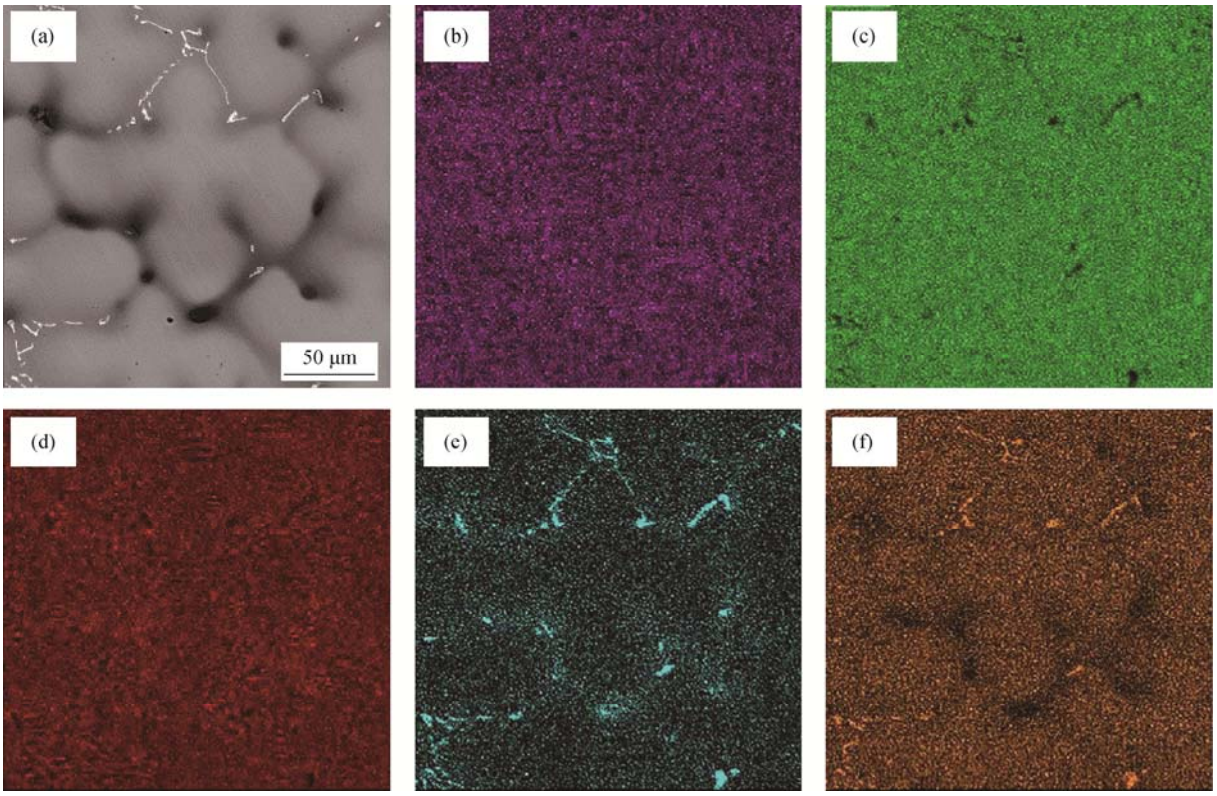

Fig. 2. SEM micrograph (a) and the corresponding X-ray mapping images of Co (b), Ni (c), Ti (d), and W (e) in the cast alloy.

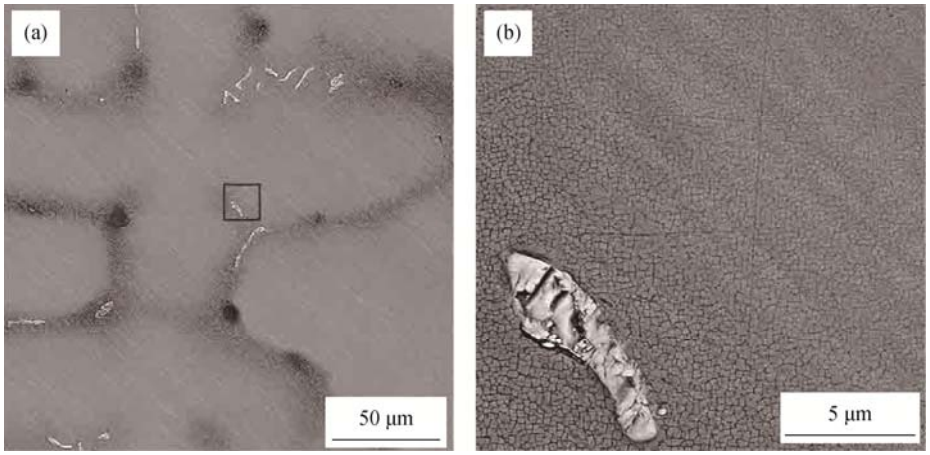

Fig. 3. Distribution of γ′-phase precipitates in the vicinity of a dendrite arm in the as-cast alloy.

Notably, in current study, the phases present in the microstructure are MC carbides, γ′ phase, and the γ matrix. No γ/γ′ eutectic regions or TCP phases were observed in the microstructure. In Ni-based superalloys, the presence of γ/γ′ eutectic structures (which have a lower melting temperature than the matrix) and TCP phases limits the applications of the alloy to lower temperatures and decreases the final properties [9,37]. Therefore, elimination of these phases is difficult or at least accompanied with some complications [38]. Anyway, the advantages of a new cast Co-based superalloy over Ni-based superalloys are the absence of unwanted phases and structures during solidification.

3.2. Effects of homogenization on segregation

The microstructures of cast and homogenized (2, 4, 8, 16, and 24 h) samples are presented in Fig. 4. The images show that, by increasing the homogenization time, the dendritic structure gradually disappears, especially after 16 h. Therefore, increasing the homogenization time at high temperature (1300°C) clearly leads to interdiffusion of atoms within the matrix because of the higher concentration of vacancies [39–40]. Thus, the coring phenomenon that occurred during the nonequilibrium casting is gradually eliminated with increasing homogenization time.

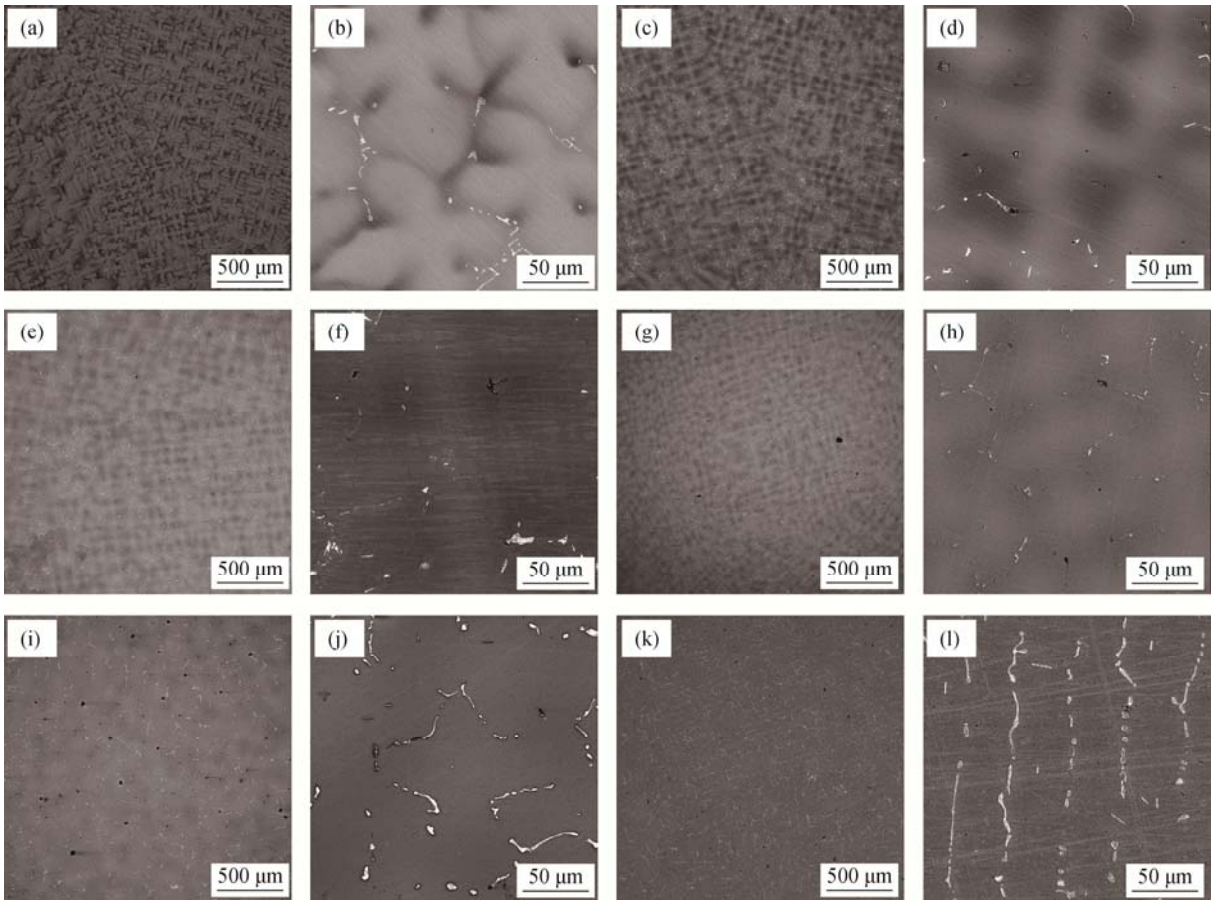

Fig. 4. SEM–BSE (backscatter electron mode) images of the alloy (a,b) in the as-cast condition and homogenized at 1300°C for different times: (c,d) 2 h; (e,f) 4 h; (g,h) 8 h; (i,j) 16 h; (k,l) 24 h.

The X-ray mapping images of the sample homogenized for 24 h are presented in Fig. 5. These images show high accumulation of Ti and W in the primary carbides, similar to the results observed for the as-cast samples (Fig. 2). This analysis shows that, in the matrix of the alloy, the main constituent elements (Co, Ni, Ti, W, and Al) are homogeneously distributed.

The average volume fractions of MC carbides in the alloy samples homogenized for 8 and 24 h were 6.5vol% and 6.4vol%, respectively. This type of carbide cannot be dissolved in the matrix at 1300°C, where they are thermodynamically stable. Some of the cast MC carbides have been reported to be stable at temperatures higher than the alloy solidus temperature [18,41].

WDS–EPMA results for the main elements of the alloy composition (Ni, Al, W, and Ti) at both the dendritic cores and the interdendritic regions are presented in Fig. 6. The difference in atomic percentage of the elements in the core of the dendrites and in the interdendritic regions decreases with increasing heat-treatment time. This result is in agreement with the microstructures presented in Fig. 4. Because the contents of Al, Ti, and Ni atoms in the interdendritic regions are higher than in the dendrite cores of the cast alloy, the atoms diffuse into regions with lower contents (i.e., the core of the dendrite). However, during homogenization, with increasing heat-treatment time, W atoms that concentrated in the core of the dendrites diffuse into the interdendritic regions (with lower W content). Fig. 4 shows that the difference between Al and Ti contents in both dendritic regions and interdendritic regions decreases substantially faster than the difference between Ni and W contents. This phenomenon is related to the higher diffusion coefficients of Al and Ti compared with those of W and Ni in the alloy matrix. This issue is discussed more thoroughly in section 3.3.

A plot of the segregation coefficient (k) as a function of the homogenization time for each element is shown in Fig. 7. The value of k is defined in Eq. (1):

$$k_{\mathrm{i}} = \frac{C_{\mathrm{i}}^{\mathrm{den.}}}{C_{\mathrm{i}}^{\mathrm{interden.}}} \tag{1}$$

where $C_{\mathrm{i}}^{\mathrm{den.}}$ and $C_{\mathrm{i}}^{\mathrm{interden.}}$ are the element content in dendritic arms and in interdendritic regions, respectively. In the alloy used in this study, the coefficients k_{Ti}, k_{Al}, k_{Ni}, and

k_W were determined as 0.3, 0.72, 0.85, and 2.19, respectively. These values indicate that W and Ti are highly segregated in the cast alloy, whereas Al and Ni are weakly segregated. The low segregation coefficients of Al and Ni may be due to the lack of a clear detection of these elements' segregation, as seen in Fig. 2. The results in Fig. 7 show that, with increasing homogenization time, the segregation coefficients for all of the elements in the alloy approach 1. This trend reveals another way of expressing the degree of elemental segregation, which decreases with increasing homogenization time, resulting in complete homogenization of the specimen.

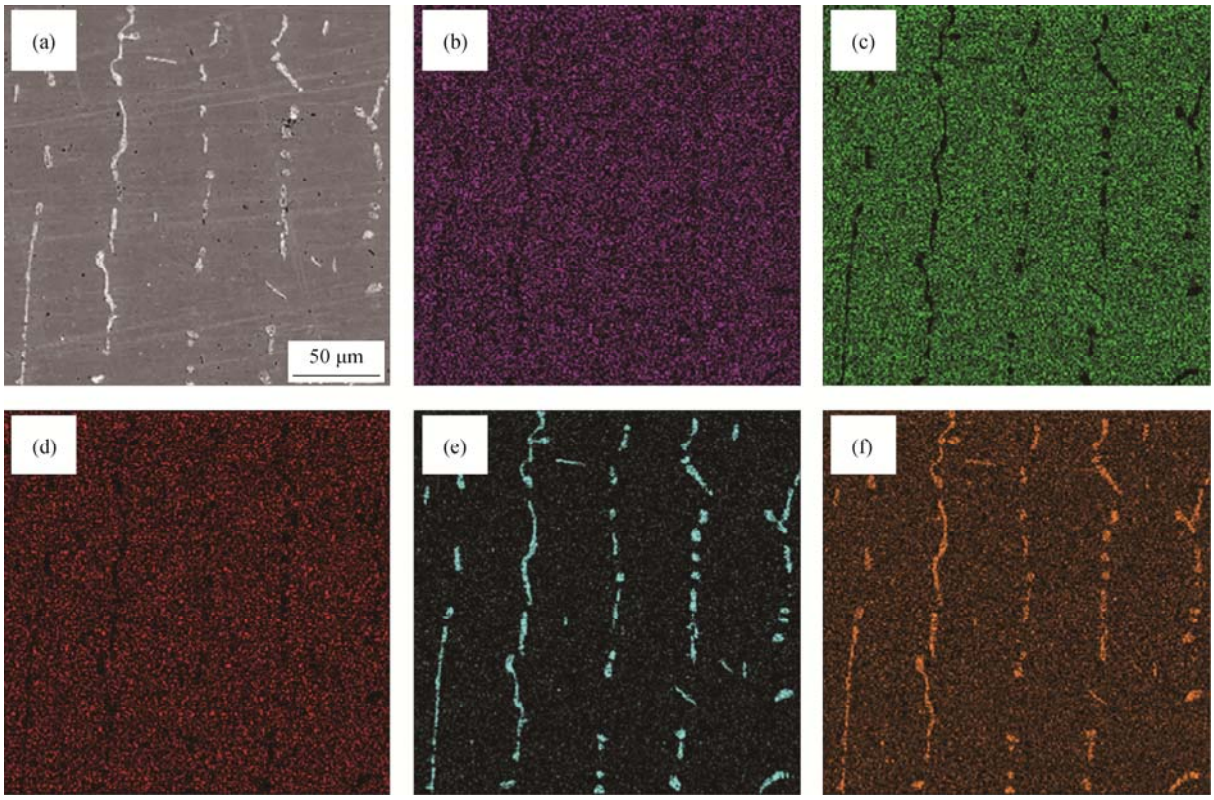

Fig. 5. SEM micrograph (a) and X-ray mapping images of Al (b), Co (c), Ni (d), Ti (e), and W (f) in the sample homogenized for 24 h.

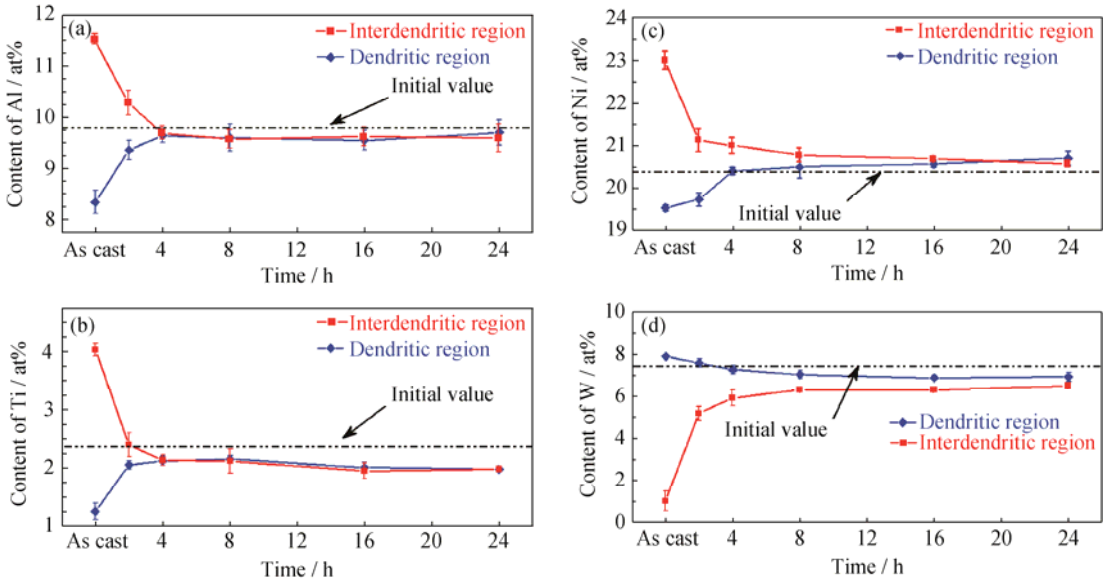

Fig. 6. Variation of the contents of elements with increasing homogenization time: (a) Al; (b) Ti; (c) Ni; (d) W.

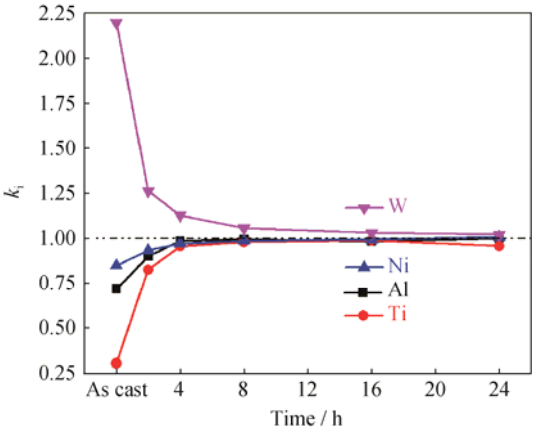

Fig. 7. Variation of the segregation coefficient (*k*) for Al, Ti, Ni, and W with increasing homogenization time.

3.3. Calculations of interdiffusion coefficient

To calculate the interdiffusion coefficient of the constituent elements during the homogenization process, we assumed that the alloy compositions follow a sinusoidal relationship [5,42]:

$$c^t = c_0 + \left(\frac{\Delta c_{\max-\min}}{2}\right)\cos\left(\frac{2\pi}{L}x\right)\exp\left(-\frac{4\pi^2}{L^2}Dt\right) \quad (2)$$

where c^t is the element content at time t, c_0 is the average element content, $\Delta c_{\max-\min}$ is the difference between the lowest and highest contents, L is the average length between the secondary dendrite arms, t is the time, and D is the volume interdiffusion coefficient. Notably, the diffusion coefficients of different elements in the alloys (interdiffusion) differ slightly from the diffusion coefficients obtained from diffusion couples [43]. Additionally, the segregation parameter (δ), which is a criterion of elemental dispersion, can be derived from the following equation (Eq. (3)):

$$\delta^t = \frac{c^t_{\max} - c^t_{\min}}{c^0_{\max} - c^0_{\min}} \quad (3)$$

Using Eqs. (2) and (3) and mathematical simplifications, a simple correlation is obtained for the determination of diffusion coefficient:

$$\ln(\delta^t) = -\frac{4\pi^2}{L^2}Dt \quad (4)$$

Using EPMA data obtained from Fig. 6 and Eq. (4), diffusion coefficients can be calculated for the principal elements, i.e., Ti, W, Al, and Ni. Notably, because of the partial homogenization after 8 h, the interdiffusion coefficients were calculated over this time; the results are displayed in Table 2. The determined values reveal that the diffusion coefficients of Al and Ti are almost two times higher than those of W and Ni. The rapid decrease in the difference between Al and Ti and the time of homogenization (see Fig. 6) can therefore be related to their higher diffusion coefficients compared with W and Ni. That is, these elements are uniformly and more rapidly diffused in the microstructure because of the higher diffusion coefficient.

Diffusion coefficients of alloy elements for several cobalt systems are presented in Table 2. A comparison of the diffusion coefficients for W (D_w) in this investigation with those reported in other studies reveals that the D_w values are very similar to those reported in most of the previously related studies (Table 2). In addition, Obata *et al*. [44] reported that the presence of W in the Co–Al–W system results in a decrease in Al diffusion coefficient. W can have a reducing effect on aluminum in these superalloys [45]. The addition of Ta to the Ni–Al–Ta system has been reported to result in a decrease of the diffusion coefficient and an increase of the diffusion activation energy [46]. Consequently, the reason for the decrease of the Al and Ti diffusion rates in the alloys used in this study is likely the high content of W and possibly Ni in the alloy (see Table 2).

3.4. Effect of segregation on the γ′-prime phase

As illustrated in Fig. 3, the sizes of the γ′ phase in the dendrite core and in the interdendritic region were very dissimilar. Also, Figs. 8(a) and 8(b) display clearly the difference in size of the γ′ phase at high magnitudes within the dendrite cores and in the interdendritic regions for the cast alloy. The average sizes of the γ′ precipitates in the

Table 2. Diffusion coefficients at 1300°C of elements in the present alloy and those reported for other Co-based alloy systems

10^{-14} m^2·s^{-1}

System	D_{Al}	D_{Ti}	D_W	D_{Ni}	Ref.
Co–Al–W–Ni–Ti	2.18	2.16	1.26	1.35	This work
Co–X	6.97	8.80	2.01	0.43	Calculated based on Ref. [40]
Co–X	16.6	19.9	1.39	—	Calculated based on Ref. [47]
Co–Al–W	17.4	—	1.54	—	Calculated based on Ref. [44]
Co–Al–W	~10	—	~1	—	Obtained from Ref. [45]
Co–Al	16.8	—	—	—	Calculated based on Ref. [48]

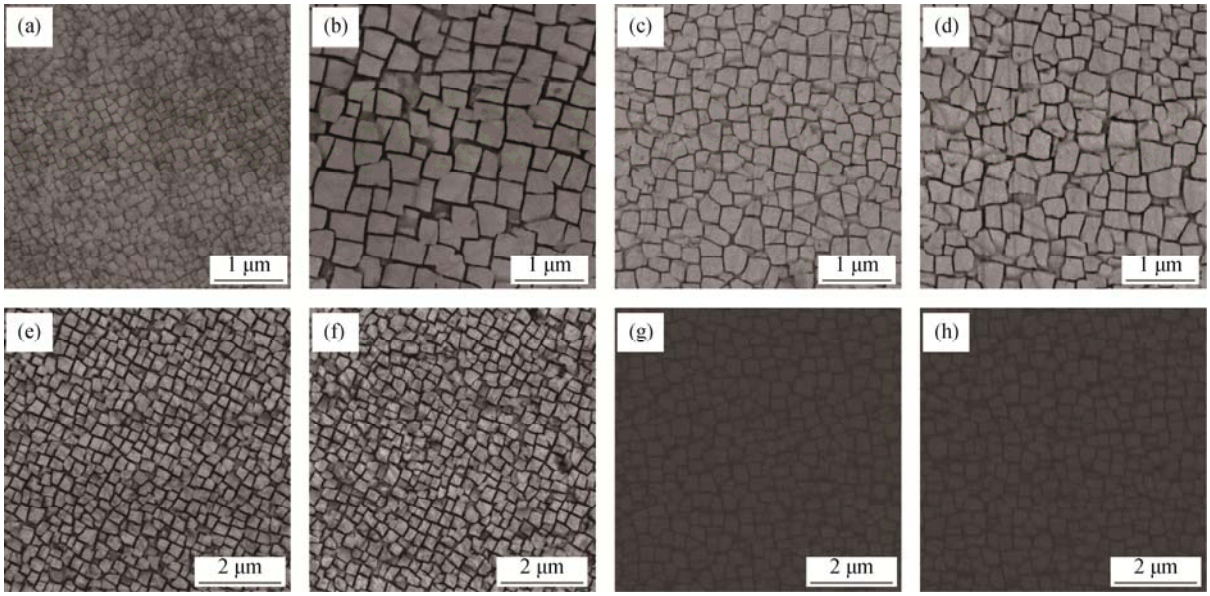

Fig. 8. The γ′-phase precipitates: (a,c,e,g) dendritic regions; (b,d,f,h) interdendritic regions; (a,b) in the as-cast condition; (c,d) homogenized for 4 h; (e,f) homogenized for 8 h; (g,h) homogenized for 16 h.

interdendritic region ($\bar{d}^{\gamma'}_{\text{interden.}}$) and in the dendrite core ($\bar{d}^{\gamma'}_{\text{den.}}$) of the cast sample were 392 and 124 nm, respectively. Microstructural images of homogenized samples after 4, 8, and 16 h of homogenization, which are presented in Fig. 8, show that, with an increase in homogenization time, the differences of γ′ sizes inside the dendrites and between the interdendrite is minimized and can be neglected. The ratio between the γ′ precipitates' size in the interdendritic regions and that in the dendrite cores ($\bar{d}^{\gamma'}_{\text{interden.}}/\bar{d}^{\gamma'}_{\text{den.}}$) for the cast sample was equal to 3.16. At the homogenization time of 4, 8, and 16 h, the $\bar{d}^{\gamma'}_{\text{interden.}}/\bar{d}^{\gamma'}_{\text{den.}}$ ratio became 1.42, 1.14, and 0.96, respectively.

WDS–EPMA analysis was carried out on some coarse γ′ precipitates in both dendrite cores and interdendritic regions. The average values of the WDS–EPMA results, which are depicted in Fig. 9, show that the sum of the Co and Ni contents is in the range of 73.7at%–77at% and that the rest of the γ′ phase comprises Al, Ti, and W. Therefore, the atomic percentage of elements in the γ′ precipitates can be correlated with the stoichiometric composition of this phase, which is $(Co,Ni)_3(Al,W,Ti)$. This result is consistent with results reported in the literature [36,49–50] about the stoichiometric compositions of γ′ particles. The important point in the chemical composition of γ′ precipitates in the cast alloy is the difference in constituent elements in dendrite cores and interdendritic regions. For example, in the cast condition, the content of Al in γ′ precipitates located in the core of dendrites was 17.1at%, whereas the amount of this element in γ′ precipitates in interdendritic regions was approximately 11.4at%. Similar trends were observed for the contents of other elements in γ′ particles, such as Ti and W, whose contents in the interdendritic and dendrite regions were 5.8at% and 1.9at% for Ti and 3.4at% and 9.7at% for W, respectively (see Fig. 9).

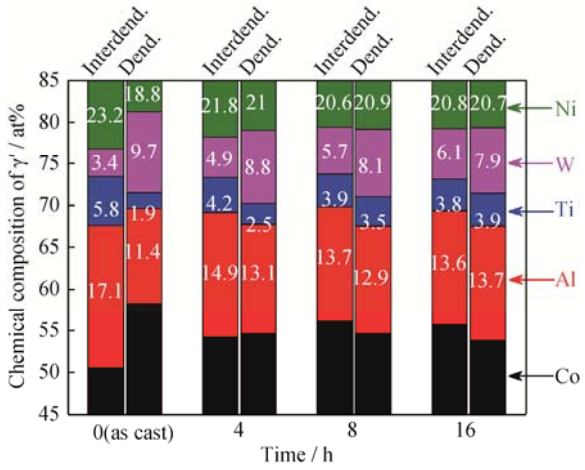

Fig. 9. Average chemical composition of γ′ phases in dendrite cores and interdendritic regions in a specimen in the as-cast condition and in specimens homogenized for 4, 8, and 16 h.

The cooling-route DSC results from cast and homogenized (4 and 16 h) samples within the temperature interval from 1200 to 1000°C are presented in Fig. 10. The precipitation temperature of γ′, which is equivalent to the onset of the initial formation of γ′ particles, is 1094°C in the cast alloy; this temperature decreases to 1074 and 1067°C after homogenization at 4 and 16 h. We attributed the precipitation temperature of γ′ to its chemical composition. Accord-

ing to the segregation of Ti at interdendritic regions (see Fig. 6) and previously reported results [51–53] that Ti can raise the precipitation temperature of the γ′ phase in Co–Al–W alloys, we concluded that the initial γ′ particles should form at interdendritic regions. Again, after a homogenization treatment and the uniform distribution of elements, especially Ti, the precipitation temperature of γ′ is decreased.

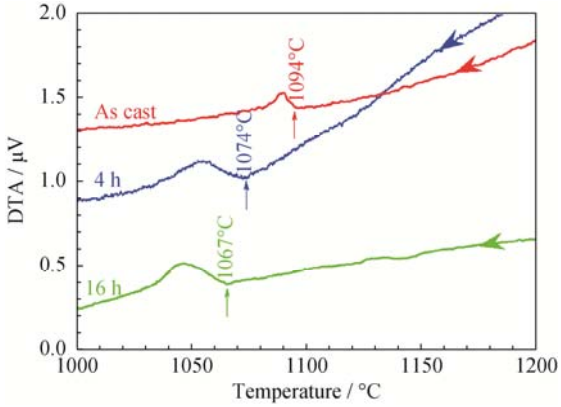

Fig. 10. Cooling-route DSC results of the cast samples homogenized for 4 and 16 h.

The variation of the microhardness of dendritic and interdendritic regions as a function of the homogenization time is presented in Fig. 11. The difference between the microhardness at the two locations is evident, especially in the as-cast sample, in which the microhardness at cores of dendrites (HV 424.6) and interdendritic regions (HV 376.7) is related to the size of the γ′ phase, which is 392 and 124 nm, respectively (Figs. 8(a) and 8(b)). With the refinement of the γ′ phase (not less than ~25 nm), the strength has been reported to increase because dislocations strongly influence the mechanism [54–55]. With increasing homogenization time, the elemental segregation decreases (Fig. 6) and the size of the γ′ phase in the two regions becomes equalized

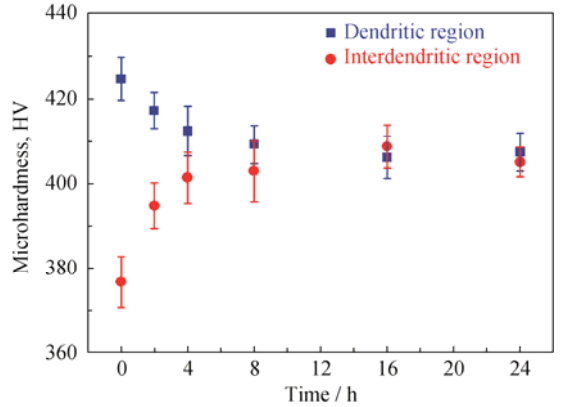

Fig. 11. Mean value of microhardness at interdendritic and dendrite regions in the cast and homogenized samples.

(Fig. 8). Fig. 8 shows that the difference between microhardness values associated with the two locations continuously approaches a horizontal asymptote of HV 405 after 8 h of homogenization.

With increasing homogenization time, the size, chemical composition, precipitation temperature, and hardness of γ′ particles in both regions become negligible (Figs. 8 and 9). This behavior can be related to several factors:

(1) Content of elements. According to Fig. 6, the contents of Ti and Al in the interdendritic region and the content of W within the dendrite core are high, especially in the as-cast sample. This difference in the elemental segregation in both locations affects the compositions of γ′ precipitates (Fig. 9). That is, the compositional difference of γ′ particles between interdendritic and dendrite regions, especially in the as-cast sample, is essentially related to the distinct constituent elements in the dendritic structure.

(2) Diffusivity. As mentioned in section 3.3, the diffusion coefficients of Ti and Al are two times greater than that of W. Moreover, according to content of constituent elements in the dendritic structure (Fig. 6), the kinetics of growth of precipitates inside interdendritic regions, where the Ti and Al contents are high, is higher than that of precipitates inside the cores. Thus, larger γ′ particles are anticipated in interdendritic regions (see Fig. 8).

(3) Precipitation temperature of γ′. Another reason for the difference in γ′ phase is attributed to this phase precipitation temperature (see Fig. 10). Apparently, γ′ particles, which form initially in interdendritic regions because of the high level of Ti in these locations, were affected by the precipitation temperature. That is, under similar cooling conditions for both regions, the γ′ particles in interdendritic regions nucleate at higher temperatures than those in the cores of the dendrites. The growth rate of γ′ in interdendrite regions is also higher than that in core locations.

The segregation of alloying elements in the cast sample affects the microstructural characteristics of γ′ precipitates. However, by homogenization, initial elemental segregation decreases so that the γ′ particles in both of the two regions can be distributed uniformly with the same characteristics. Finally, according to the aforementioned results of the compression mechanical tests at 850°C, the proof yield strength of the sample homogenized for 16 h was (708 ± 3) MPa.

4. Conclusions

(1) Microstructures of the cast and homogenized new γ/γ′ Co-based superalloy contained MC carbides (rich in Ti and W) and γ′ phase with a stoichiometric composition of

$(Co,Ni)_3(Al,W,Ti)$ and was free from detrimental phases and γ/γ′ eutectics structures.

(2) In the cast alloy, Al, Ni, and Ti elements segregated mainly in interdendritic regions, whereas W was mainly segregated in dendrite cores, irrespective of the amount of W that appeared in the interdendrite regions in the form of carbides.

(3) Homogenizing the cast alloy at 1300°C eliminates the core structure, causing a uniform dispersion of elements and eliminating the segregation, especially after 16 h.

(4) The sizes, chemical composition, and microhardness of the γ′ phase in the cast alloy in the dendrite cores and in the interdendritic regions differed. These differences were attributed to the segregation of elements in these regions.

(5) Homogenization treatment by reducing segregation causes a uniform dispersion of γ′ phase in the microstructure having the same characteristics.

(6) Interdiffusion coefficients of primary elements (Al, W, Ni, and Ti) at 1300°C were calculated in this study. The results show that interdiffusion coefficients of Al and Ti are approximately two times higher than those of W and Ni.

Acknowledgement

The authors would like to appreciate the support of Dr. Jahanafrooz for this research.

References

[1] V.A. Wills and D.G. McCartney, A comparative study of solidification features in nickel-base superalloys: Microstructural evolution and microsegregation, *Mater. Sci. Eng. A*, 145(1991), No. 2, p. 223.

[2] N. Warnken, D. Ma, A. Drevermann, R.C. Reed, S.G. Fries, and I. Steinbach, Phase-field modelling of as-cast microstructure evolution in nickel-based superalloys, *Acta Mater.*, 57(2009), No. 19, p. 5862.

[3] G.D. Merz, T.Z. Kattamis, and A.F. Giamei, Microsegration and homogenization of Ni–7.5wt%Al–2.0wt%Ta dendritic monocrystals, *J. Mater. Sci.*, 14(1979), No. 3, p. 663.

[4] M.S.A. Karunaratne, D.C. Cox, P. Carter, and R.C. Reed, Modelling of the microsegregation in CMSX-4 superalloy and its homogenisation during heat treatment, *Superalloys*, 2000, p. 263.

[5] Z.J. Miao, A.D. Shan, Y.B. Wu, J. Lu, W.l.. Xu, and H.W. Song, Quantitative analysis of homogenization treatment of INCONEL718 superalloy, *Trans. Nonferrous Met. Soc. China*, 21(2011), No. 5, p. 1009.

[6] Y.J. Li, Y.F. Teng, X.H. Feng, and Y.S. Yang, Effects of pulsed magnetic field on microsegregation of solute elements in a Ni-based single crystal superalloy, *J. Mater. Sci. Technol.*, 33(2017), No. 1, p. 105.

[7] J.B. le Graverend, J. Cormier, P. Caron, S. Kruch, F. Gallerneau, and J. Mendez, Numerical simulation of γ/γ′ microstructural evolutions induced by TCP-phase in the MC2 nickel base single crystal superalloy, *Mater. Sci. Eng. A*, 528(2011), No. 6, p. 2620.

[8] A.S. Golezani, M. Bageri, and R. Samadi, Microstructural change, and impact toughness property of Inconel 738LC after 12 years of service, *Eng. Fail. Anal.*, 59(2016), p. 624.

[9] M.R. Jahangiri, S.M.A. Boutorabi, and H. Arabi, Study on incipient melting in cast Ni base IN939 superalloy during solution annealing and its effect on hot workability, *Mater. Sci. Technol.*, 28(2012), No. 12, p. 1402.

[10] S.H. Fu, J.X. Dong, M.C. Zhang, and X.S. Xie, Alloy design and development of INCONEL718 type alloy, *Mater. Sci. Eng. A*, 499(2009), No. 1-2, p. 215.

[11] Y.Z. Zhou and A. Volek, Effect of carbon additions on hot tearing of a second generation nickel-base superalloy, *Mater. Sci. Eng. A*, 479(2008), No. 1-2, p. 324.

[12] C.N. Wei, H.Y. Bor, and L. Chang, The effects of carbon content on the microstructure and elevated temperature tensile strength of a nickel-base superalloy, *Mater. Sci. Eng. A*, 527(2010), No. 16-17, p. 3741.

[13] F. Long, Y.S. Yoo, C.Y. Jo, S.M. Seo, Y.S. Song, T. Jin, and Z.Q. Hu, Formation of η and σ phase in three polycrystalline superalloys and their impact on tensile properties, *Mater. Sci. Eng. A*, 527(2009), No. 1-2, p. 361.

[14] J. Zhang and R.F. Singer, Effect of Zr and B on castability of Ni-based superalloy IN792, *Metall. Mater. Trans. A*, 35(2004), No. 4, p. 1337.

[15] A. Epishin, T. Link, U. Brückner, B. Fedelich, and P. Portella, Effects of segregation in nickel-base superalloys: Dendritic stresses, *Superalloys*, 2004, p. 537.

[16] P. Li, S.S. Li, and Y.F. Han, Influence of solution heat treatment on microstructure and stress rupture properties of a Ni_3Al base single crystal superalloy IC6SX, *Intermetallics*, 19(2011), No. 2, p. 182.

[17] M.T. Kim, D.S. Kim, and O.Y. Oh, Effect of γ′ precipitation during hot isostatic pressing on the mechanical property of a nickel-based superalloy, *Mater. Sci. Eng. A*, 480(2008), No. 1-2, p. 218.

[18] D.L. Sponseller, Differential thermal analysis of nickel-base superalloys, *Superalloys*, 1996, p. 259.

[19] D.A. Porter and K.E. Easterling, *Phase Transformations in Metals and Alloys*, 2nd Ed., CRC Press, State of Florida, 1992, p. 61.

[20] F.J. Humphreysand M. Hatherly, *Recrystallization and Related Annealing Phenomena*, Elsevier, The Netherlands, 2004, p. 137.

[21] J. Sato, T. Omori, K. Oikawa, I. Ohnuma, R. Kainuma, and K. Ishida, Cobalt-base high-temperature alloys, *Science,*

312(2006), No. 5770, p. 90.

[22] K. Tanaka, M. Ooshima, N. Tsuno, A. Sato, and H. Inui, Creep deformation of single crystals of new Co–Al–W-based alloys with fcc/$L1_2$ two-phase microstructures, *Philos. Mag.*, 92(2012), No. 32, p. 4011.

[23] M.S. Titus, A. Suzuki, and T.M. Pollock, Creep and directional coarsening in single crystals of new γ–γ′ cobalt-base alloys, *Scripta Mater.*, 66(2012), No. 8, p. 574.

[24] F. Xue, H.J. Zhou, X.H. Chen, Q.Y. Shi, H. Chang, M.L. Wang, X.F. Ding, and Q. Feng, Creep behavior of a novel Co–Al–W-base single crystal alloy containing Ta and Ti at 982°C, *MATEC Web of Conferences*, 14(2014), p. 15002.

[25] A. Bauer, S. Neumeier, F. Pyczak, R.F. Singer, and M. Göken, Creep properties of different γ′-strengthened Co-base superalloys, *Mater. Sci. Eng. A*, 550(2012), p. 333.

[26] S. Neumeier, L.P. Freund, and M. Göken, Novel wrought γ/γ′ cobalt base superalloys with high strength and improved oxidation resistance, *Scripta Mater.*, 109(2015), p. 104.

[27] A. Suzuki and T.M. Pollock, High-temperature strength and deformation of γ/γ′ two-phase Co–Al–W-base alloys, *Acta Mater.*, 56(2008), No. 6, p. 1288.

[28] M. Tsunekane, A. Suzuki, and T.M. Pollock, Single-crystal solidification of new Co–Al–W-base alloys, *Intermetallics*, 19(2011), No. 5, p. 636.

[29] X.F. Ding, T. Mi, F. Xue, H.J. Zhou, and M.L. Wang, Microstructure formation in γ–γ′ Co–Al–W–Ti alloys during directional solidification, *J. Alloys Compd.*, 599(2014), p. 159.

[30] E.T. McDevitt, Feasibility of cast and wrought Co–Al–WX gamma-prime superalloys, *Mater. Sci. Forum*, 783-786(2014), p. 1159.

[31] I. Lopez-Galilea, C. Zenk, S. Neumeier, S. Huth, W. Theisen, and M. Göken, The thermal stability of intermetallic compounds in an as-cast SX Co-base superalloy, *Adv. Eng. Mater.*, 17(2015), No. 6, p. 741.

[32] J. Koßmann, C.H. Zenk, I. Lopez-Galilea, S. Neumeier, A. Kostka, S. Huth, W. Theisen, M. Göken, R. Drautz, and T. Hammerschmidt, Microsegregation and precipitates of an as-cast Co-based superalloy—microstructural characterization and phase stability modelling, *J. Mater. Sci.*, 50(2015), No. 19, p. 6329.

[33] P.J. Bocchini, E.A. Lass, K.W. Moon, M.E. Williams, C.E. Campbell, U.R. Kattner, D.C. Dunand, and D.N. Seidman, Atom-probe tomographic study of γ/γ′ interfaces and compositions in an aged Co–Al–W superalloy, *Scripta Mater.*, 68(2013), No. 8, p. 563.

[34] F. Pyczak, A. Bauer, M. Göken, U. Lorenz, S. Neumeier, M. Oehring, J. Paul, N. Schell, A. Schreyer, A. Stark, and F. Symanzik, The effect of tungsten content on the properties of $L1_2$-hardened Co–Al–W alloys, *J. Alloys Compd.*, 632(2015), p. 110.

[35] H.Y. Yan, V.A. Vorontsov, and D. Dye, Alloying effects in polycrystalline γ′ strengthened Co–Al–W base alloys, *Intermetallics*, 48(2014), p. 44.

[36] K. Shinagawa, T. Omori, J. Sato, K. Oikawa, I. Ohnuma, R. Kainuma, and K. Ishida, Phase equilibria and microstructure on γ′ phase in Co–Ni–Al–W system, *Mater. Trans.*, 49(2008), No. 6, p. 1474.

[37] R.C. Kramb, M.M. Antony, and S.L. Semiatin, Homogenization of a nickel-base superalloy ingot material, *Scripta Mater.*, 54(2006), No. 9, p. 1645.

[38] S.R. Hegde, R.M. Kearsey, and J.C. Beddoes, Designing homogenization–solution heat treatments for single crystal superalloys, *Mater. Sci. Eng. A*, 527(2010), No. 21-22, p. 5528.

[39] A. Janotti, M. Krčmar, C.L. Fu, and R.C. Reed, Solute diffusion in metals: Larger atoms can move faster, *Phys. Rev. Lett.*, 92(2004), No. 8, p. 85901.

[40] S.S. Naghavi, V.I. Hegde, and C. Wolverton, Diffusion coefficients of transition metals in fcc cobalt, *Acta Mater.*, 132(2017), p. 467.

[41] L. Gong, B. Chen, Z.H. Du, M.S. Zhang, R.C. Liu, and K. Liu, Investigation of solidification and segregation characteristics of cast Ni-base superalloy K417G, *J. Mater. Sci. Technol.*, 34(2016), No. 3, p. 541.

[42] X.L. Pan, H.Y. Yu, G.F. Tu, W.R. Sun, and Z.Q. Hu, Segregation and diffusion behavior of niobium in a highly alloyed nickel-base superalloy, *Trans. Nonferrous Met. Soc. China*, 21(2011), No. 11, p. 2402.

[43] Y. Minamino, Y. Koizumi, N. Tsuji, T. Yamada, and T. Takahashi, Interdiffusion in Co solid solutions of Co–Al–Cr–Ni system at 1423 K, *Mater. Trans.*, 44(2003), No. 1, p. 63.

[44] S. Obata, M. Moniruzzaman, and Y. Murata, Interdiffusion in Co-based Co–Al–W ternary alloys at elevated temperatures, *ISIJ Int.*, 54(2014), No. 10, p. 2129.

[45] H. Chang, G.L. Xu, X.G. Lu, L. Zhou, K. Ishida, and Y.W. Cui, Experimental and phenomenological investigations of diffusion in Co–Al–W alloys, *Scripta Mater.*, 106(2015), p. 13.

[46] J. Chen, L. Zhang, J. Zhong, W. Chen, and Y. Du, High-throughput measurement of the composition-dependent interdiffusivity matrices in Ni-rich fcc Ni–Al–Ta alloys at elevated temperatures, *J. Alloys Compd.*, 688(2016), p. 320.

[47] S. Neumeier, H.U. Rehman, J. Neuner, C.H. Zenk, S. Michel, S. Schuwalow, J. Rogal, R. Drautz, and M. Göken, Diffusion of solutes in fcc cobalt investigated by diffusion couples and first principles kinetic Monte Carlo, *Acta Mater.*, 106(2016), p. 304.

[48] A. Green and N. Swindells, Measurement of interdiffusion coefficients in Co–AI and Ni–AI systems between 1000 and 1200°C, *Mater. Sci. Technol.*, 1(1985), No. 2, p. 101.

[49] I. Povstugar, P.P. Choi, S. Neumeier, A. Bauer, C.H. Zenk,

M. Göken, and D. Raabe, Elemental partitioning and mechanical properties of Ti- and Ta-containing Co–Al–W-base superalloys studied by atom probe tomography and nanoindentation, *Acta Mater.*, 78(2014), p. 78.

[50] I. Povstugar, C.H. Zenk, R. Li, P.P. Choi, S. Neumeier, O. Dolotko, M. Hoelzel, M. Göken, and D. Raabe, Elemental partitioning, lattice misfit and creep behaviour of Cr containing γ′ strengthened Co base superalloys, *Mater. Sci. Technol.*, 32(2016), No. 3, p. 220.

[51] V.A. Vorontsov, J.S. Barnard, K.M. Rahman, H.Y. Yan, P.A. Midgley, and D. Dye, Coarsening behaviour and interfacial structure of γ′ precipitates in Co–Al–W based superalloys, *Acta Mater.*, 120(2016), p. 14.

[52] C.H. Zenk, S. Neumeier, H.J. Stone, and M. Göken, Mechanical properties and lattice misfit of γ/γ′ strengthened Co-base superalloys in the Co–W–Al–Ti quaternary system, *Intermetallics*, 55(2014), p. 28.

[53] A. Bauer, S. Neumeier, F. Pyczak, and M. Göken, Microstructure and creep strength of different γ/γ′-strengthened Co-base superalloy variants, *Scripta Mater.*, 63(2010), No. 12, p. 1197.

[54] M.J. Donachie and S.J. Donachie, *Superalloys: A Technical Guide*, ASM international, New York, 2002, p. 82.

[55] R.C. Reed, *The Superalloys: Fundamentals and Applications*, Cambridge University Press, Cambridge, 2008, p. 216.